Microporous and Mesoporous Materials 195 (2014) 2–8

Contents lists available at ScienceDirect

Microporous and Mesoporous Materials

journal homepage: www.elsevier.com/locate/micromeso

Facile synthesis of biocompatible superparamagnetic mesoporous nanoparticles for imageable drug delivery

Tuomo Nissinen [a], Simo Näkki [a], Mika Latikka [b], Markku Heinonen [c], Timo Liimatainen [d], Wujun Xu [a], Robin H.A. Ras [b], Olli Gröhn [d], Joakim Riikonen [a], Vesa-Pekka Lehto [a],*

[a] Department of Applied Physics, University of Eastern Finland, 70211 Kuopio, Finland
[b] Department of Applied Physics, Aalto University, 02150 Espoo, Finland
[c] Department of Physics and Astronomy, University of Turku, 20014 University of Turku, Finland
[d] A.I. Virtanen Institute for Molecular Science, University of Eastern Finland, 70211 Kuopio, Finland

ARTICLE INFO

Article history:
Received 5 December 2013
Received in revised form 21 March 2014
Accepted 5 April 2014
Available online 13 April 2014

Keywords:
Mesoporous silicon
Iron oxide
Nanocomposite
Nanoparticles
Biomedicine

ABSTRACT

Superparamagnetic mesoporous silicon nanoparticles have a huge potential in drug delivery and diagnostics, i.e., in theranostics. These particles can carry high drug payloads, they can be targeted by external magnetic fields, they can be imaged by magnetic resonance imaging and they are biocompatible. In the present study, we demonstrate a fast and simple synthesis procedure to produce superparamagnetic mesoporous nanoparticles by precipitating iron oxide nanocrystals inside the pores of porous silicon. Subsequently, polyethylene glycol molecules with two different molecular sizes were conjugated onto the external surfaces of the composite nanoparticles to improve the colloidal stability of the suspension without compromising the magnetic properties of the composite. The developed nanoparticles possessed many advantageous properties such as superparamagnetic behavior, high T_2 relaxivity, high pore volume and modifiable surface chemistry. In addition, the present method is more straightforward and versatile than the previous methods published, preserving the pore volume larger and accessible for high drug loadings.

1. Introduction

Mesoporous (pore diameter 2–50 nm) drug delivery systems have stimulated considerable interest in the scientific community [1]. Mesoporous silicon (PSi) is a feasible material, since it has many desirable features such as biocompatibility [2], a modifiable surface [3–5] and high porosity, with a controllable and uniform pore size distribution as well as large surface area. The large pore volume of PSi particles enables loading of therapeutics into the pores and the mesopores can protect the payload molecules from both chemical and enzymatic degradation [6]. The pore walls can also be modified chemically in order to achieve the desired interaction between the pore walls and the drug molecules thereby controlling the release of the drug [7,8]. Triggered release of pharmaceuticals by external stimulus has also been demonstrated [9].

Superparamagnetic iron oxide nanoparticles (SPION), are considered to be both biocompatible and safe material [10,11], and their applications in biomedicine have been investigated extensively in recent years. Superparamagnetism is an important feature, because without the presence of an external magnetic field the particles will not agglomerate, since they do not have any remanent magnetization. These, typically magnetite (Fe_3O_4) or maghemite (γ-Fe_2O_3), particles have been shown to clearly shorten the transverse relaxation times (T_2) of surrounding water molecules through the outer sphere relaxation mechanism. This feature makes them traceable by magnetic resonance imaging (MRI) and thus beneficial for diagnostic applications [12–14]. In addition, magnetically targeted drug delivery has been investigated with promising results [15–17].

Magnetic porous nanoparticles can combine the benefits of the mesoporous materials and SPIONs, therefore, having huge potential in biomedical applications. These nanoparticles can be produced by incorporating magnetic material into the PSi matrix. This has been previously done by trapping prefabricated SPIONs inside the pores with a method utilizing oxidation of the PSi surface to expand the PSi matrix, while fixing the SPIONs inside the pores [18,19]. However, drawback with this method is that the pores can become blocked by the SPIONs from both ends and a large part of the pore volume becomes inaccessible. The use of oxidation is mandatory here and this may also impose some restrictions on the surface modifications and further on the processability of the material.

---

* Corresponding author. Tel.: +358 40 355 2470.
E-mail address: vesa-pekka.lehto@uef.fi (V.-P. Lehto).

http://dx.doi.org/10.1016/j.micromeso.2014.04.014
1387-1811/

Coating of nanoparticles to increase their so called stealth properties against the body's reticuloendothelial system is an essential part of designing drug delivery systems. Typically, plain nanoparticles have too brief times in the blood circulation to have useful diagnostic or drug delivery applications [20]. Polyethylene glycol (PEG) coating of the external surface of the particles has been used to decrease blood protein binding and macrophage uptake and thus to prolong the biological half-life in blood [21].

In the present study, iron oxide nanocrystals with superparamagnetic behavior and high T_2 relaxivity (r_2) were precipitated inside the pores of PSi nanoparticles with a novel technique. The detailed illustration of the developed method is presented in Scheme 1. In the method, the only restriction on the surface chemistry is the hydrophilicity of the pore walls. This enables an expanded range of different surface functionalizations such as thermal carbonization resulting in slower biodegradation of the material [22]. This might be useful for applications requiring longer treatment times. Decrease of the pore volume is also anticipated to be less with the previous technique.

Two types of PEG molecules with different molecular size were successfully conjugated on the surface of the PSi/iron oxide composite nanoparticles. This dual PEGylation improved the colloidal stability of the nanoparticles in ionic solution better that could be achieved with one sized PEG, which is common procedure. The dual PEGylation was developed also to increase the lifetime of the nanoparticles in the blood circulation *in vivo*. The effect of the dual PEGylation to r_2 was also investigated in this study.

2. Experimental

2.1. Chemicals and materials

Silicon wafers (p+, (100), 0.01–0.02 Ω/cm) were obtained from Siegert Wafer GmbH. Ethanol (99.5%) was purchased from Altia Oyj. Hydrofluoric acid (HF) 38–40% and *n*-hexane were purchased from Merck. $FeCl_3·6H_2O$ and $FeCl_2·4H_2O$ were acquired from Sigma–Aldrich and 24.5% NH_4OH and buffer solution from J.T. Baker. 2 kDa methoxy-PEG-silane and 0.5 kDa methoxy-PEG-silane were purchased from Laysan Bio Inc. and ABCR GmbH respectively.

2.2. Preparation of the composite

PSi films were prepared by etching p+ type silicon wafers in the HF/EtOH mixture (1:1). Details of the production of the PSi films have been described elsewhere [4]. The films were ground in a planetary ball mill in ethanol and the nanoparticles were separated from the suspension by centrifugation. The separated particles were dried and thermally oxidized in air at 300 °C for 2 h. In order to increase the density of OH groups on the surface, the particles were further chemically oxidized by immersing them in a 1:1:6 solution of H_2O_2:HCl:H_2O for 15 min at 85 °C. The produced PSi-OH particles were washed three times with deionized water and dried.

To produce PSi/iron oxide composite nanoparticles (FeO/PSi-OH), 100 mg of particles with the pore volume of 0.82 cm^3/g were immersed in hexane and 120 μL of deoxygenated (by N_2-bubbling) aqueous solution containing 2 M Fe^{3+} and 1 M Fe^{2+} ions was added with vigorous stirring (Scheme 1). The particles were then separated from hexane and dried in the oven at 85 °C to remove water from the pores. After drying, the particles were immersed again in hexane and 480 μL of 24.5% aqueous ammonia was added. The suspension was left to react at room temperature for 20 min, which after the particles were washed 3 times with deionized water and dried at 65 °C.

Finally, the particles were covalently coated with PEG to form the PEGylated PSi/iron oxide composite (FeO/PSi-OH-PEG). 250 mg of 2 kDa methoxy-PEG-silane and 400 μL of 0.5 kDa methoxy-PEG-silane were dissolved in 5 ml toluene and then 50 mg of the particles were immersed in PEG solution and the system was deoxygenated with N_2 bubbling for 20 min. The reaction was conducted overnight with a reflux method at 120 °C. Subsequently, the mixture was dried and the particles were washed and ultrasonicated five times in ethanol and five times in deionized water.

2.3. Characterization

The iron content of samples was examined with atomic absorption spectroscopy (AAS). An Analytic Jena AAS ZEEnit 700 device was used at a wavelength of 248.3 nm. Dried particles were dissolved with microwave dissolution oven in the following acids: nitric acid, hydrochloric acid, hydrofluoric acid and boric acid. Thermogravimetry (TG) (TA Q50 TGA) was used to measure the amount of PEG conjugated to the surface of the particles. The samples were heated prior to the actual measurement at 65 °C for 1 h and the measurements were performed from 65 °C to 600 °C at a heating rate of 10 °C/min in 200 l/min N_2 flow.

The particle size and ζ-potential were measured in a suspension with deionized water or phosphate buffered saline (PBS) with a Malwern Zetasizer Nano ZS instrument. The *Z*-average size was measured with 173° backscattering configuration and the Huckel approximation was used for calculating the ζ-potential. The effect

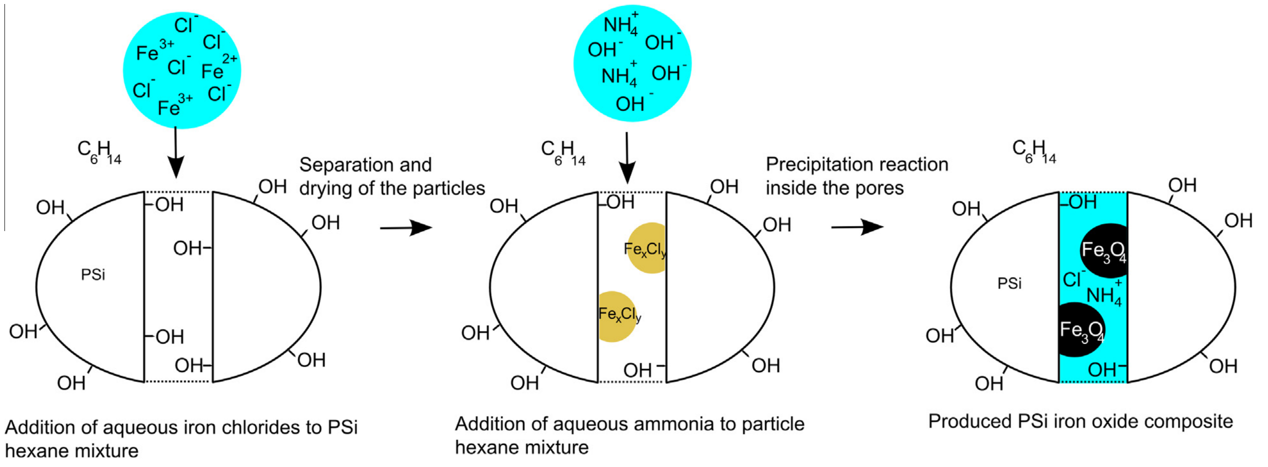

Addition of aqueous iron chlorides to PSi hexane mixture

Addition of aqueous ammonia to particle hexane mixture

Produced PSi iron oxide composite

Scheme 1. Illustration of the precipitation of iron oxide into the pores of the porous silicon nanoparticle.

of surface coating on the colloidal stability was investigated by incubating both FeO/PSi-OH and FeO/PSi-OH-PEG nanoparticles in PBS with the size of the particles being monitored over time.

The porous structure was characterized by N_2 sorption (Micromeritics TriStar II 3020) at 77 K. The dried particles were measured three times for each sample. The surface area, A, was calculated from adsorption branch using BET (Brunaer, Emmett and Teller) theory, pore volume, V, from single point at $p/p_0 = 0.98$ and average pore diameter, D, with the equation $D = 4V/A$.

X-ray powder diffraction (XRPD) was used to investigate the crystal structure of the iron oxide in the samples. A Bruker D8 Dixcover powder diffractometer was used with a Cu K_α radiation source at 40 kV and 40 mA for range 25–110° of 2θ. The measurements time was 16 h with the Ni filter in front of the detector. The average crystallite size of iron oxides was calculated with Bruker Topas software by using the Scherrer equation for the Rietveld-fitted data. The fundamental parameter method was used to estimate the effect of the instrumental broadening of the diffraction peaks.

Oxidation states of iron ions were examined by measuring the Fe 2p and 3p peaks with X-ray photoelectron spectroscopy (XPS) using Perkin-Elmer PHI 5400 for measurements with Al K_α radiation. The charging effect was corrected by assuming that the O S1 peak associated with iron existed at an energy value of 530 eV. Multiplet peak fitting was used for Fe $2p_{2/3}$ peak to determine the ratio between different iron oxides. Peak parameters were obtained from literature [23,24] and 0.6 eV was added to FWHM for each component because of the different resolution used for the measurement. Unifit software was used for fitting.

JEOL JEM2100F transmission electron microscope (TEM) with an acceleration voltage of 200 kV was used to study the size and morphology of the nanoparticles. The samples were prepared by drying a drop of aqueous particle suspension on Formvar coated 200 mesh copper TEM grid.

Magnetic properties were investigated with a Quantum Design MPMS-XL 7 Tesla superconductive quantum interference device (SQUID). Approximately 10 mg of sample powder was sealed in Kapton tape and placed in a standard polypropylene straw sample holder. The background due to the sample holder and Kapton tape was removed using the background subtraction option in the Quantum Design software. Hysteresis loops were measured with reciprocating sample configuration with 8 mm amplitude and 4 Hz frequency between -7 and $+7T$ at room temperature. Magnetizations were measured per the total masses of the samples.

For magnetic resonance relaxation measurements 9.4T vertical magnet (Oxford Instruments, Plc, Witney, UK) interfaced to the Varian DirectDrive console (Agilent Technologies, Palo Alto, CA) was used. For the RF transmit and receive, a quadrature 10 mm volume coil was used (Rapid Biomed, Rimpar, Germany). All relaxation measurements were conducted from whole sample volume (0.5 ml) at room temperature. In the longitudinal relaxation time (T_1) measurements, inversion recovery sequence was applied with 7 inversion times varying between 0.125 s and 6 s depending on the relaxation time. The spin echo sequence was applied for T_2 measurements with the echo time ranging between 0.008 s and 6 s. Several measurements to optimize inversion time and/or echo time were needed for samples at the extremities of relaxation times. The average of two measurements was used for each sample. The MRI relaxivities were calculated per mass of iron (provided by the AAS measurements).

3. Results

The iron content of the FeO/PSi-OH sample was 11.1% (w/w) as measured with AAS. Due to the PEGylation the mass of the particles increased by 25% (w/w) and the relative mass of iron decreased to 4.7% (w/w). The relative decrease of the iron mass could not be totally explained by the additional mass of PEG molecules, but approximately 45% of the iron oxide nanocrystals were lost during the extensive washing and ultrasonication procedure needed for the removal of the unconjugated PEG.

The success of PEGylation was confirmed by measuring the size and ζ-potential of the nanoparticles in aqueous suspensions. PEGylation is known to reduce the absolute value of ζ-potential and to improve the stability of particle suspensions, especially in ionic solutions. Accordingly, PEGylation of particles changed their ζ-potential from -38 mV to -8 mV. All the particle size and ζ-potential results are presented in Table 1. In the measurements, all the samples were separated by centrifugation with identical parameters. PEGylation increased the hydrodynamic diameter of the FeO/PSi-OH particles from 162 nm to 277 nm, partly because of the water molecules bonded around the particles which increased the average hydrodynamic diameter of them and partly because of the lower density of the PEGylated particles which decreased the their sedimentation speed during centrifugation.

XRPD was used to investigate the crystal structure of PSi-OH and FeO/PSi-OH samples (Fig. 1). The diffraction peaks measured for PSi-OH were consistent with the ICCD data of silicon (PDF 00-027-1402). After the precipitation of iron oxide, two new broad low-intensity peaks could be observed at 2θ angles of 35.6° and 63.0°. According to the ICCD database, structures of Fe_3O_4 (PDF 00-019-0629) and γ-Fe_2O_3 (PDF 00-039-1346) (Fig. 2) provided the best match with the new peaks with γ-Fe_2O_3 producing a slightly better fit. The four most intensive peaks of γ-Fe_2O_3 and all silicon peaks were fitted to the measured data by Rietveld refinement and the crystallite size of 4.0 nm for iron oxide was obtained. The fitting is presented at Supplementary Information Fig. S1.

XPS was used to further investigate the phase of the iron oxide. Fe 2p and Fe 3p peaks of sample FeO/PSi-OH (Fig. 2) were compared to the literature references [23,25]. Both Fe^{2+} and Fe^{3+} oxidation states can be observed from Fe $2p_{2/3,}$ since there was no clear satellite peak typical for pure Fe^{3+} at 719 eV binding energy or satellite at 715 eV typical for pure Fe^{2+}. Also Fe $2p_{2/3}$ and Fe 3p

Table 1

Compilation of the results for the samples PSi-OH, FeO/PSi-OH and FeO/PSi-OH-PEG.

Sample	Surface area[a] (m^2/g)	Pore volume/Si mass[b] (cm^3/g)	Pore diameter[c] (nm)	Iron content[d] (% w/w)	ζ-Potential[e] (mV)	Particle diameter[f] (nm)	T_2 relaxivity[g] ($mM^{-1}\,s^{-1}$)
PSi-OH	163 ± 8	0.82 ± 0.03	20 ± 1	0	−52 ± 8	164	0
FeO/PSi-OH	228 ± 0	0.52 ± 0.01	9 ± 0	11.1	−38 ± 2	162	240
FeO/PSi-OH-PEG	16 ± 4	0.14 ± 0.03	35 ± 11	4.7	−8 ± 5	277	231

[a] Surface area calculated from N_2-isotherm (mean ± std, $n = 3$).

[b] Single point pore volume per mass of silicon calculated similarly.

[c] Pore size calculated from earlier results with equation $d = 4\,V/A$, where A is surface area and V is pore volume.

[d] Iron content measured by atomic adsorption spectroscopy.

[e] Mean ζ-potential of nanoparticles in DI-water suspension and std ($n = 3$) measured with electrophoretic light scattering.

[f] Z-average of hydrodynamic diameter of particle determined by dynamic light scattering.

[g] T_2 relaxivity measured with MRI in deionized water.

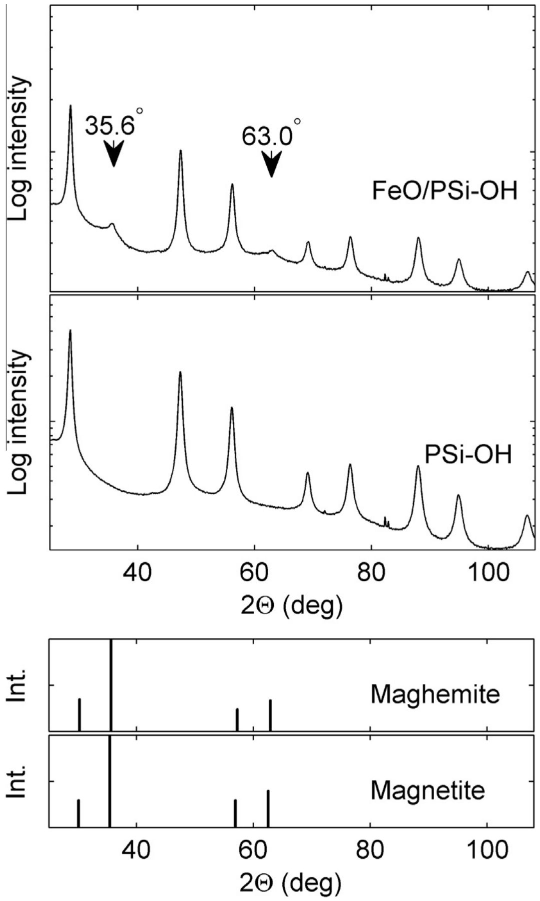

Fig. 1. XRPD diffractograms of FeO/PSi-OH composite and PSi-OH as well as the four most intensive peaks of maghemite and magnetite according to ICCD database (PDF 00-019-0629 and PDF 00-039-1346).

peaks were slightly broaden to lower energy values indicating presence of Fe^{2+}. Multiplet structures of Fe_3O_4 and γ-Fe_2O_3 were fitted to measured Fe 2p$_{2/3}$ peak, in order determine the ratio between them. Result of 44% for Fe_3O_4 and 56% for γ-Fe_2O_3 were obtained. The fitting and obtained parameters are presented at Supplementary information Fig. S2 and Table S1.

The single point pore volumes and the BET surface areas were obtained from the N_2 sorption isotherms (Supplementary Information Fig. S3). In order to estimate the loss of the pore volume due to iron oxide precipitation and PEGylation, the volumes were calculated per mass of PSi. The results are presented in Table 1. The surface area and pore volume of the PEGylated particles were unrealistically low as will be discussed later. The drug loading and release capacity of non-PEGylated particles was also examined to show the accessibility of the pore for cargo molecules (Supplementary Information Fig. S4).

TEM was used to examine the morphology and the structure of the FeO/PSi-OH-PEG sample. The black parallel lines can be seen on the particle image (Fig. 3a. These lines represent the iron oxides crystals inside the parallel pores of the PSi nanoparticle. Similar lines have also been observed in composite nanoparticles produced by trapping method [18]. The porous structure can be observed in Fig. 3b showing a particle full of 10–20 nm voids. Iron oxides can be seen only in the thinnest particles, because contrast was lost with thicker particles that excessively absorbed electrons. Larger TEM images are presented in Supplementary Information Fig. S5 and S6 to give overview of the particles.

The magnetization curves (Fig. 4a and b) obtained with the SQUID magnetometer showed negligible hysteresis and both paramagnetic (positive susceptibility at high fields) and superparamagnetic (high initial susceptibility) behavior. Superparamagnetic saturation magnetizations were calculated per the mass of the iron in the samples (provided by AAS measurements) by subtracting the linear paramagnetic component from the data, resulting in 8.6 emu/(g Fe) for FeO/PSi-OH and 10.0 emu/(g Fe) for FeO/PSi-OH-PEG.

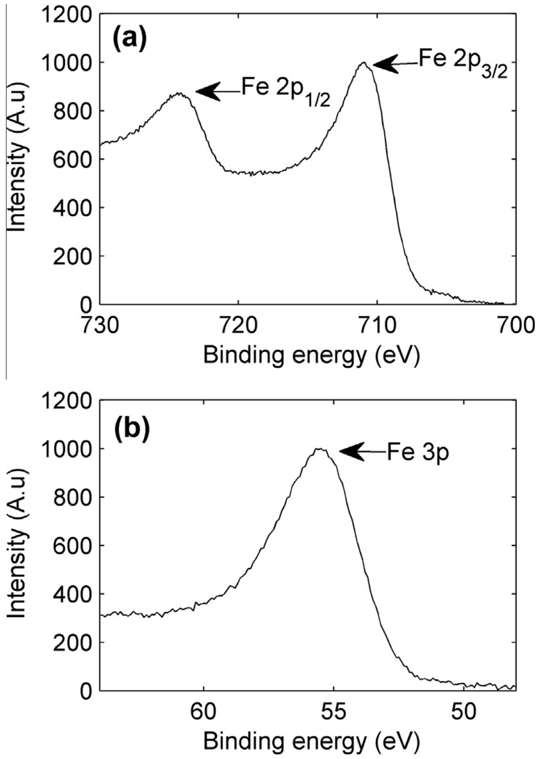

Fig. 2. (a) XPS Fe 2p peaks for FeO/PSi-OH sample. (b) XPS Fe 3p peak for FeO/PSi-OH sample.

MRI relaxivities were measured to investigate suitability of the particles for MRI imaging. T_1 relaxivity (r_1) not observed for any of the samples or either the r_2 for the PSi-OH. The r_2 values for FeO/PSi-OH and FeO/PSi-OH-PEG were 240 mM^{-1} s^{-1} and 231 mM^{-1} s^{-1} respectively, calculated from relaxivity curves (Fig. 4c). The effect of the permanent magnet on the particles FeO/PSi-OH particles in water is shown in Fig. 4d.

In order to determine the stability of composite nanoparticle suspensions, the particles were incubated in PBS buffer and the hydrodynamic diameter was monitored with DLS (Fig. 5) for 160 h. The hydrodynamic diameter of FeO/PSi-OH-PEG particles was stable for at least 3 days whereas non-PEGylated FeO/PSi-OH agglomerated fast after incubation. This also verified the successful PEGylation.

4. Discussion

4.1. Preparation of composite

The aim of the present study was to develop an alternative method for producing PSi iron oxide composite nanoparticles that would be simpler and more versatile as compared to the previously reported method. The trapping method introduced by Kinsella et al. [18] represented a successful approach, but it suffered from pore blocking that decreased the porosity from 86% to 35%. Especially for drug delivery purposes, a high pore volume and a large surface area are one of the most crucial properties, since they largely define the loading capacity of the porous carrier. Therefore,

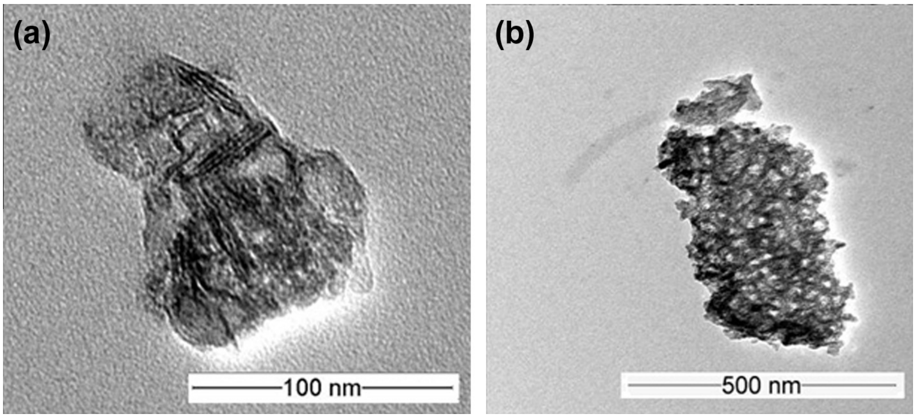

Fig. 3. TEM photographs of the FeO/PSi-OH-PEG nanoparticles.

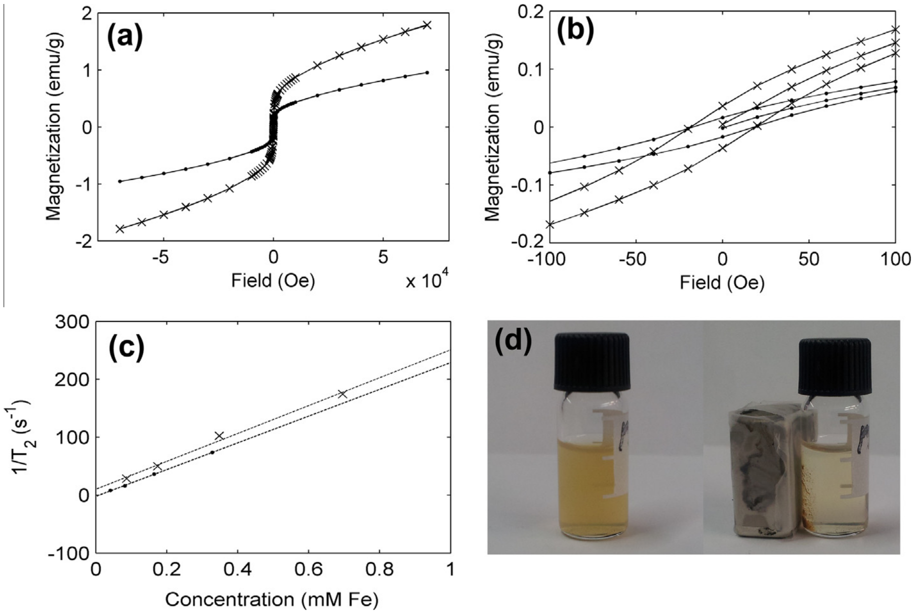

Fig. 4. (a) Magnetization curves of FeO/PSi-OH (**crosses**) and FeO/PSi-OH-PEG (**dots**) per the total masses of the samples. (b) Zoomed part of the magnetization curve. (c) T_2 Relaxivity curves of FeO/PSi-OH (**crosses**) and FeO/PSi-OH-PEG (**dots**). (d) The effect of a permanent magnet on the FeO/PSi-OH nanoparticles in water.

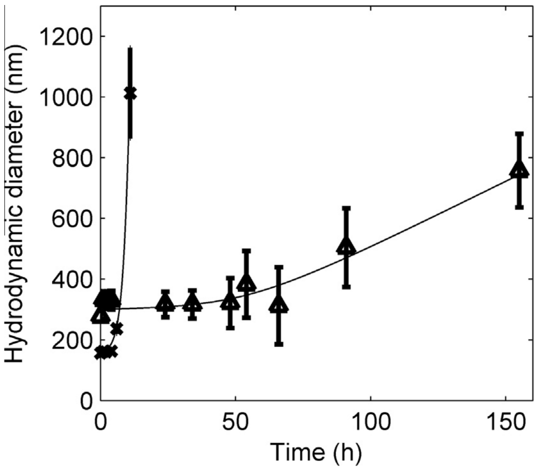

Fig. 5. Hydrodynamic diameter of FeO/PSi-OH (**crosses**) and FeO/PSi-OH-PEG (**triangles**) nanoparticles stored in PBS buffer.

one important goal in the present research was to prevent pore blocking and the resulting decrease in porosity in the composite nanoparticles. The so-called two solvent method (i.e., reactants are soluble in one solvent but insoluble in the other) was used to drive reactants into the pores and prevent iron oxide crystal formation on the outer surface of the particles [26]. The precipitation method developed was based on the following rationale (Scheme 1).

First, a hydroxyl-terminated, negatively charged and hydrophilic surface was generated by oxidizing the PSi nanoparticles both thermally and chemically. Thermal oxidation was applied to produce a thick oxide layer on the pore surfaces to stabilize the particles and chemical oxidation was then applied in order to maximize the density of OH groups and, therefore, to increase the hydrophilicity of the surface. Oxidation of the PSi has been examined in detail in our previous research [5] and it has been also postulated that the hydroxyl terminated PSi surface is a suitable substrate for deposition of iron oxide [27]. The oxidized particles were first immersed in the non-polar solvent hexane after which aqueous iron chloride solution with a volume equal to the pore volume of the PSi was added to the mixture. Because of the presence of the hydrophilic pore walls, iron chloride solution was driven inside the pores by polar interactions. Particles were dried in order to evaporate the water and crystallize the iron chlorides in the pores. Subsequently, the dried particles were immersed in hexane and ammonium hydroxide was added. The aqueous ammonium hydroxide was also driven into the pores by polar interactions, and there was dissolution of iron chlorides with the simultaneous precipitation of iron oxide.

$$2Fe^{3+} + Fe^{2+} + 8OH^- \rightarrow Fe_3O_4 + 4H_2O$$

which occurred at high pH values (>9) [28]. The particles were washed several times and dried after which PEG-silane molecules were covalently bonded to the hydroxyl terminated surface of the PSi with silane coupling.

According to the formula above the expected form of iron oxide is Fe_3O_4. In our case both Fe_3O_4 and γ-Fe_2O_3 were present with approximated ratio of 44/56. Forming of γ-Fe_2O_3 was likely caused by oxidation of Fe^{2+} ions by free oxygen that has not completely eliminated from the reaction. Also originally formed Fe_3O_4 could have also been oxidized partially to γ-Fe_2O_3 when particles were stored in air. Fe_3O_4 is known to be oxidized to γ-Fe_2O_3 without any passivating chemical coating in the presence of oxygen [29]. If homogenious phase of iron oxide is needed for certain application, Fe_3O_4 could be oxidized completely to γ-Fe_2O_3 at elevated temperatures.

4.2. Composition and structure

As mentioned above, small superparamagnetic iron oxide crystals could be precipitated on the pore walls of PSi. The average crystal size of 4.0 nm was estimated by the Rietveld refinement. Typically 10–40 nm diameter iron oxide nanoparticles can be produced with the precipitation method [30], but special conditions, such as an elevated temperature or a use of surfactant, are needed to produce smaller particles [31]. The small crystal size of iron oxide indicates that the small pore size had limited the crystal growth. If grown on the external surface of silicon particles the iron oxide crystals would have grown larger spontaneously. The location of the nanocrystals was verified with the TEM studies. This approach can also be utilized in the production of ultra-small iron oxide nanocrystals.

Precipitation of iron oxide into the pores decreased the pore volume only by 37% from 0.82 cm^3/g to 0.52 cm^3/g and correspondingly the pore size declined from 20 nm to 9 nm. The presence of iron oxide in the pores, decreased the volume as expected, but the porosity was still acceptable for cargo loading. The pores were not totally blocked and the decrease of porosity was less than that occurring with the trapping method [18]. The crystallite size of iron oxide was small enough not to block pores effectively since the initial pore size was calculated to be 20 nm and crystallite size of the iron oxides was only ca. 4 nm.

PEGylation decreased both the BET surface area and the pore volume significantly. PEG covers mesoporous channels after drying the particles for N_2 sorption measurement as shown in the previous study [32]. This behavior is very likely responsible for the low values of pore volume and surface area, especially since the PEG content was as high as 25% (w/w). Despite the large decrease in the pore volume of the dry particles, it is likely that the pores will be accessible when in an aqueous suspension of PEG-FeO/PSi nanoparticles. The high r_2 value in relaxivity experiments supports this assumption, since blockade of the pores would hinder water diffusion into the pores and if that occurred the r_2 value of PEGylated sample would decrease considerably.

4.3. Magnetic properties

The SQUID measurements suggested that there was a paramagnetic component in the magnetization of the composite nanoparticles, because magnetization was not saturated at high magnetic fields. The small iron oxide crystals have a high surface to volume ratio and therefore there are a relatively high amount of iron atoms on the surface layer. The paramagnetic component was likely caused by the unpaired spins of electrons of the surface atoms, since no other chemical components were observed by XRPD or XPS. This type of paramagnetic surface layer has been previously observed for SPIONs of few nanometer sizes [33].

Because of the small crystallite size of iron oxide, the magnetic moments of single iron oxide crystals were low and the saturation magnetization of the bare FeO/PSi-OH composite remained low (8 emu/(Fe g)). Typically SPIONs have a crystal size between 5 and 20 nm and saturation between 20 and 50 emu/(Fe g) depending on the crystal size and the spatial separation of particles [28]. Since the saturation magnetization is calculated per mass of iron, PEGylation has typically a non-significant effect on saturation magnetization. Accordingly, there was only a minor difference in the saturation values between plain and PEGylated nanoparticles.

According to the outer sphere theory, r_2 is proportional to the square of the saturation magnetization and to the square of core the radius of the magnetic particle [34]. With the trapping method a value of 555 $nM^{-1}\ s^{-1}$ was obtained for the weighted T_2 relaxivity (r_2^*). The measured r_2 value of FeO/PSi-OH (240 $nM^{-1}\ s^{-1}$) was still high and when considering the low saturation magnetization, this was particularly interesting result. The values of r_2^* is always higher than the non-weighted counterpart r_2 and therefore the relaxivity difference between the trapping and the precipitation methods would be actually even lower. The r_2 of FeO/PSi should be much lower than 240 $nM^{-1}\ s^{-1}$ when taking into account both the small crystal size and the low saturation magnetization. Hence there must be some other mechanism that can affect the r_2 value. One possible explanation according to the outer sphere theory is that diffusion of water near the iron oxide crystals was significantly faster for the FeO/PSi composites obtained than for the composite manufactured by the trapping method. The open pores allowed better diffusion, since water molecules could move freely inside the pores.

Coating of superparamagnetic nanoparticles with macromolecules has generally a major effect on the r_2 value, since the coating hinders the water diffusion around the surface of the iron oxide crystals or immobilizes nearby water atoms by hydrogen bonding [35]. Nevertheless, dual PEGylation seemed to exert only a minor effect on the r_2 value, most likely because the PEG-coating was mainly on the external surface of Fe/PSi composite nanoparticles permitting the easy diffusion of water molecules inside the pores near to the iron oxide crystals. The dual PEGylation seems to be very promising coating method to obtain magnetic nanoparticles for MRI applications.

4.4. Colloidal stability

PEGylation has been shown to prevent protein binding, because of the hydration layer and steric repulsion between proteins and the PEG molecules. Generally, macrophage uptake is the main mechanism for removal of nanoparticles from the blood circulation [21]. Macrophage uptake results from the binding of serum proteins to the nanoparticles, a property determined by the surface chemistry and the size of the nanoparticles [36]. Therefore, the improved colloidal stability in ionic dispersions also improved the stealth properties against the reticuloendothelial system, since larger particle clusters will tend to bind more proteins, leading to more effective macrophage uptake.

5. Conclusions

We have developed a novel method to incorporate ultrafine iron oxide crystals by precipitation into the pores of PSi nanoparticles. The form of the iron oxide was mixture of Fe_3O_4 and γ-Fe_2O_3 (ratio 9/11) with the crystallite size of 4.0 nm possessing superparamagnetic properties. After precipitation, the pore volume of the nanoparticles declined only by 37%, remaining large enough to allow storage of material for drug delivery applications. The measured r_2 (240 $nM^{-1}\,s^{-1}$) was especially high considering the low saturation magnetization (8 emu/g Fe) and the crystallite size.

The novel precipitation method is simple and versatile allowing also utilization of thermally carbonized porous silicon surfaces for incorporation of iron oxide nanocrystals.

Dual PEGylation was found to prevent the particle agglomeration in PBS buffer and exerted only a minor effect on the MRI properties of the particles ($r_2 = 231\ nM^{-1}\,s^{-1}$). Therefore, the mesoporous superparamagnetic nanoparticles prepared with the precipitation method have potential *in vivo* MRI applications, thus making them promising candidate as theranostic device.

Acknowledgement

The research has been supported by the strategic funding of University of Eastern Finland.

Appendix A. Supplementary data

Supplementary data associated with this article can be found, in the online version, at http://dx.doi.org/10.1016/j.micromeso.2014.04.014.

References

[1] W. Xu, J. Riikonen, V.-P. Lehto, Int. J. Pharm. 253 (2013) 181–197.
[2] L.T. Canham, Adv. Mater. 7 (1995) 1033–1037.
[3] W. Xu, J. Riikonen, T. Nissinen, M. Suvanto, K. Rilla, B. Li, et al., J. Phys. Chem. C 116 (2012) 22307–22314.
[4] L.M. Bimbo, M. Sarparanta, H.A. Santos, A.J. Airaksinen, E. Makila, T. Laaksonen, et al., ACS Nano 4 (2010) 3023–3032.
[5] J. Riikonen, M. Salomäki, J. van Wonderen, M. Kemell, W. Xu, O. Korhonen, et al., Langmuir 28 (2012) 10573–10583.
[6] A.R. Zimmerman, J. Chorover, K.W. Goyne, S.L. Brantley, Environ. Sci. Technol. 38 (2004) 4542–4548.
[7] J. Salonen, L. Laitinen, A. Kaukonen, J. Tuura, M. Björkqvist, T. Heikkilä, et al., J. Control. Release 108 (2005) 362–374.
[8] M. Kovalainen, J. Mönkäre, E. Mäkilä, J. Salonen, V-P. Lehto, K. Herzig, et al., Pharm. Res. 29 (2012) 837–846.
[9] L.A. Perelman, C. Pacholski, Y.Y. Li, M.S. Van Nieuwenhze, M.J. Sailor, Nanomedicine 3 (2008) 31–43.
[10] S. Hussain, K. Hess, J. Gearhart, K. Geiss, J. Schlager, Toxicol. In Vitro 19 (2005) 975–983.
[11] D. Ling, T. Hyeon, Small (2012).
[12] J.E. Rosen, L. Chan, D. Shieh, F.X. Gu, Biol. Med. 8 (2012) 275–290.
[13] M. Corti, A. Lascialfari, M. Marinone, A. Masotti, E. Micotti, F. Orsini, et al., J. Magn. Mater. 320 (2008) e316–e319.
[14] C. Haw, F. Mohamed, C. Chia, S. Radiman, S. Zakaria, N. Huang, et al., Ceram. Int. 36 (2010) 1417–1422.
[15] B. Chertok, B.A. Moffat, A.E. David, F. Yu, C. Bergemann, B.D. Ross, et al., Biomaterials 29 (2008) 487–496.
[16] A.S. Lübbe, C. Alexiou, C. Bergemann, J. Surg. Res. 95 (2001) 200–206.
[17] C. Alexiou, R.J. Schmid, R. Jurgons, M. Kremer, G. Wanner, C. Bergemann, et al., Eur. Biophys. J. 35 (2006) 446–450.
[18] J.M. Kinsella, S. Ananda, J.S. Andrew, J.F. Grondek, M. Chien, M. Scadeng, et al., Adv. Mater. 23 (2011) H248–H253.
[19] L. Gu, J. Park, K.H. Duong, E. Ruoslahti, M.J. Sailor, Small 6 (2010) 2546–2552.
[20] J.V. Jokerst, T. Lobovkina, R.N. Zare, S.S. Gambhir, Nanomedicine 6 (2011) 715–728.
[21] A.S. Karakoti, S. Das, S. Thevuthasan, S. Seal, Angew. Chem. Int. Ed. 50 (2011) 1980–1994.
[22] J. Salonen, A.M. Kaukonen, J. Hirvonen, J. Pharm. Sci. 97 (2008) 632–653.
[23] S.R. Chowdhury, E.K. Yanful, A.R. Pratt, J. Hazard. Mater. (2012).
[24] M.C. Biesinger, B.P. Payne, A.P. Grosvenor, L.W. Lau, A.R. Gerson, R.S.C. Smart, Appl. Surf. Sci. 257 (2011) 2717–2730.
[25] T. Yamashita, P. Hayes, Appl. Surf. Sci. 254 (2008) 2441–2449.
[26] M. Imperor-Clerc, D. Bazin, M. Appay, P. Beaunier, A. Davidson, Chem. Mater. 16 (2004) 1813–1821.
[27] S. Balakrishnan, Y.K. Gun'ko, T.S. Perova, R.A. Moore, M. Venkatesan, A.P. Douvalis, et al., Small 2 (2006) 864–869.
[28] A.K. Gupta, M. Gupta, Biomaterials 26 (2005) 3995–4021.
[29] S. Sun, H. Zeng, J. Am. Chem. Soc. 124 (2002) 8204–8205.
[30] K. Petcharoen, A. Sirivat, Mater. Sci. Eng. B 177 (2012) 421–427.
[31] J. Lee, T. Isobe, M. Senna, J. Colloid Interface Sci. 177 (1996) 490–494.
[32] Q. He, J. Zhang, J. Shi, Z. Zhu, L. Zhang, W. Bu, et al., Biomaterials 31 (2010) 1085–1092.
[33] J.Y. Park, P. Daksha, G.H. Lee, S. Woo, Y. Chang, Nanotechnology 19 (2008) 365603.
[34] P. Gillis, F. Moiny, R.A. Brooks, Magn. Res. Med. 47 (2002) 257–263.
[35] S. Tong, S. Hou, Z. Zheng, J. Zhou, Nano Lett. 10 (2010) 4607–4613.
[36] C.D. Walkey, J.B. Olsen, H. Guo, A. Emili, W.C. Chan, J. Am. Chem. Soc. 134 (2012) 2139–2147.